Spin Fano Resonances and Control in Two-Dimensional Mesoscopic Transport

Chen-Rong Liu,[1] Liang Huang,[1,*] Honggang Luo,[1,2] and Ying-Cheng Lai[3,4]

[1] *School of Physical Science and Technology, and Key Laboratory for Magnetism and Magnetic Materials of MOE, Lanzhou University, Lanzhou, 730000 Gansu, China*

[2] *Beijing Computational Science Research Center, 100084 Beijing, China*

[3] *School of Electrical, Computer, and Energy Engineering, Arizona State University, Tempe, Arizona 85287, USA*

[4] *Department of Physics, Arizona State University, Tempe, Arizona 85287, USA*

(Received 12 August 2019; revised manuscript received 27 January 2020; accepted 28 February 2020; published 25 March 2020)

In electronic transport through mesoscopic systems, the various resonances in quantities such as conductance and scattering cross sections are characterized by the universal Fano formula. Does a similar formula exist for spin transport? We provide an affirmative answer by deriving a Fano formula to characterize the resonances associated with two fundamental quantities underlying spin transport: spin-resolved transmission and the spin polarization vector. In particular, we generalize the conventional Green's function formalism to spin transport and use the Fisher-Lee relation to obtain the spin-resolved transmission matrix, which enables the spin polarization vector to be calculated, leading to a universal Fano formula for spin resonances. Particularly, the theoretically obtained resonance width depends on the nature of the classical dynamics as determined by the geometric shape of the dot. We explicitly demonstrate this fact and argue that it can be used to smooth out or even eliminate Fano spin resonances by manipulating the classical dynamics, which can be realized by applying or withdrawing a properly designed local gate potential. Likewise, modulating the classical dynamics in a different way can enhance the resonance. This is of particular importance in the design of electronic switches that can control the spin orientation of the electrons associated with the output current through weakening or enhancement of a Fano resonance, which are a key component in spintronics.

DOI: 10.1103/PhysRevApplied.13.034061

I. INTRODUCTION

The Fano formula was proposed in 1961 [1] to explain the sharply asymmetric profile experimentally observed in the absorption spectrum of Rydberg atoms [2]. A general form of the formula describing the resonance profile can be written as

$$\sigma = \frac{(\epsilon + q)^2}{1 + \epsilon^2}, \tag{1}$$

where σ is a measurable quantity such as the spectral intensity, the scattering cross section, or the conductance, ϵ is the amount by which the normalized energy deviates from the center of the resonance defined to be $\epsilon = 0$, and q is a parameter characterizing the degree of asymmetry of the resonance that is essential for experimental fitting of the resonance profile. In particular, for $q \neq 1$, the resonance profile is asymmetric because the quantity σ attains a maximum value at $\epsilon = 1/q$ and a minimum value at $\varepsilon = -q$. Fano resonances arise in scattering and transport processes, and the validity of the formula has been established in a variety of two-dimensional (2D) electronic transport processes in mesoscopic systems [2–11], for example, quantum dots [12,13], and Anderson impurity systems [14]. In terms of quantum information, the Fano peaks correspond to the so-called "einselection" states [15–17].

For electronic transport through a quantum-dot structure, the geometric shape of the dot (or scattering) region determines the particular type of classical dynamics, for example, integrable, mixed (nonhyperbolic), or chaotic, and can affect the resonance profile [18]. In particular, for integrable or nonhyperbolic dynamics, there are stable periodic orbits in the dot region, in which a classical trajectory can be trapped indefinitely (i.e., with an infinite lifetime). In the corresponding quantum system, if the energy (or wave number) of the electron is such that the geometric distance along a stable periodic orbit is an integer multiple of the wavelength, constructive interference arises, leading to a quantum resonance at the particular energy. Since the classical lifetime along a resonant stable periodic orbit is infinite, in principle the quantum resonance will be infinitely sharp, which, however, cannot occur due to the effect of wave dispersion. Nonetheless,

*huangl@lzu.edu.cn

the resonance can be sharp. Owing to the existence of various stable periodic orbits in the system with different orbital length, sharp resonances can occur at a discrete set of energies [19–22], corresponding to the einselection states [7,15,17]. In contrast, for fully developed chaotic classical dynamics within the dot region, all periodic orbits are unstable, reducing significantly the quantum dwell time and broadening the corresponding resonance profile. From a different perspective, the resonance peak and width, for example,, in an electronic transport system, can be used to detect and distinguish the corresponding classical dynamics [18] and to analyze wave coherence [20–22]. There have been studies on characterizing or controlling quantum coherence through Fano resonance [3,6,23–25].

A vast majority of the previous work on Fano resonance in mesoscopic transport systems focused on electronic properties such as conductance, with spin largely ignored. In spintronics applications [26,27], the spin degree of freedom of electrons plays a fundamental role. An issue of applied value is whether Fano resonances can arise in spin transport in 2D mesoscopic systems. In this regard, there have been studies on the spin-dependent Fano effect or resonance in electronic transport characteristics such as conductance [21,23,28–38]. In particular, the feasibility of performing single-spin readout in a quantum dot based on Fano resonance in conductance was studied [28], the interplay between the Fano effect and Rashba spin-orbit interaction in an Aharanov-Bohm ring coupled with quantum-dot systems was investigated [23,29–31], and Fano-like backscattering leading to dips in the channel conductance was used for spin filtering [32]. In addition, spin filtering based on Fano resonances in open quantum-dot systems was suggested [33]. It was also found that inelastic spin-dependent electron scattering by a magnetic impurity and a spin dimer leading to spin flip can induce Fano resonances in the transport characteristics [34]. Spin interference and the Fano effect in electron transport through a mesoscopic ring side-coupled with a quantum dot [35] and spin-dependent Fano resonance induced by a conducting chiral helimagnet in a quasi-one-dimensional electron waveguide [36] have been investigated. Spin filters and Fano antiresonances in conductance in a polymer device were studied by the nonequilibrium Green's function approach [37]. The spin-dependent Fano effect in a T-shaped double quantum dot was used to achieve perfect spin polarization [38]. All previous efforts in this area were concerned with the effect of spin on Fano resonances in conductance (i.e., the spin-dependent Fano effect). Our focus is on Fano resonances in quantities directly characterizing spin, not on how different spin orientations affect Fano resonances in electronic properties such as conductance. A pertinent open question is whether a universal formula as Eq. (1) exists to characterize the Fano resonances in spin transport. To our knowledge, a systematic and mechanistic understanding of Fano resonances in physical quantities defined directly in terms of spin is lacking, and the goal of this work is to develop such an understanding. Quantitatively, we analyze two fundamental quantities underlying spin transport: spin-resolved transmission and the spin polarization vector, and derive a Fano formula for both.

Concretely, we concentrate on spin transport through 2D quantum-dot systems with Rashba spin-orbit interaction and preserved time-reversal symmetry. To be as general as possible, we choose the dot geometry such that the classical dynamics are of the mixed type [39–44], where the phase space contains both Kolmogorov-Arnold-Moser (KAM) tori and chaotic regions. As the system is open, classically there is transient chaos or chaotic scattering of a nonhyperbolic nature [45]. Technically, our method to derive a Fano formula for spin transport is as follows. We first generalize the conventional Green's function to spin transport. We then use the Fisher-Lee relation [4,24] to obtain the spin-resolved transmission matrix, which enables the spin polarization vector to be calculated. The end result of the calculation is a Fano-like formula in terms of the spin polarization vector. Finally, we study the effect of the geometric shape of the dot (or the nature of classical dynamics) on spin transport and articulate a spin control scheme. Before our work, a Fano-like formula for spin transport did not exist and, as we demonstrate, our study has pertinent applied value in spintronics in terms of controlling or manipulating spin transport.

II. NONHYPERBOLIC QUANTUM-DOT SYSTEM AND THE SPIN POLARIZATION VECTOR

We study quantum-dot systems with a bow-shaped type of scattering region, as shown in Fig. 1(a). In the mesoscopic regime, representative parameter values are radius $R = 0.6$ μm and the cut width $w = 0.7R$ (so the chord length $l = 2d = 2\sqrt{R^2 - w^2}$), and s is the arc length of the upper circular section. We attach two identical leads of height $h = 0.2R$: one to the left end and the other to the right end of the open cavity. In the lead, there are $N = 12$ transverse modes at most. Rashba spin-orbit interaction exists in the shaded region [46] with an electric field $\mathbf{E}$ applied perpendicular to the cavity plane. Figure 1(b) illustrates the structure of the classical phase space on the Poincaré surface of section in terms of the Birkhoff coordinates [47] of the corresponding closed billiard system. There is a mixture of KAM tori and a chaotic sea [48], signifying nonhyperbolic dynamics [45].

An effective approach to modulating spin transport is to create a large KAM island in the classical phase space so as to generate strong quantum localized states that lead to sharp Fano resonances, which can be broken by tuning

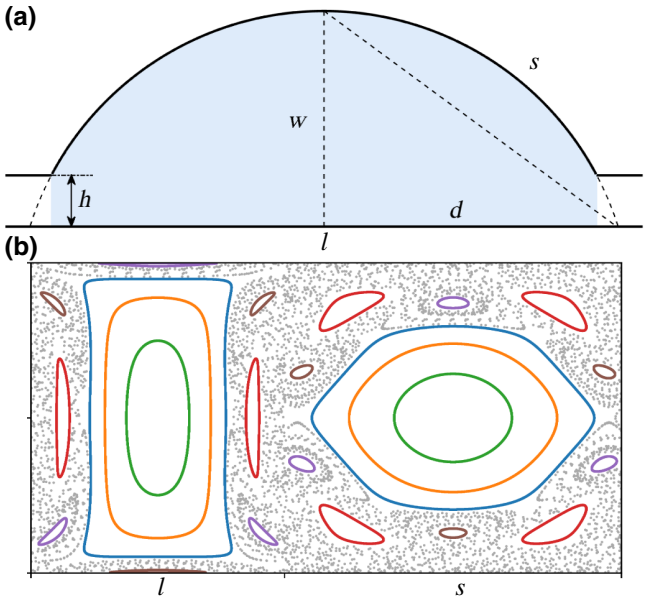

FIG. 1. The bow-shaped dot geometry and the phase-space structure on the Poincaré surface of section. (a) Geometry of the quantum dot: a bow-shaped open cavity with two leads, one attached to the left end and another to the right end. The geometric parameters are radius $R = 0.6\ \mu$m and cut width $w = 0.7R$. The height of the lead $h = 0.2R$, which permits $N = 12$ transverse modes. (b) Poincaré surface of section of the corresponding closed-cavity system in terms of the Birkhoff coordinates. The classical dynamics are mixed or nonhyperbolic.

an externally controllable parameter. We test the scenario to generate a circular forbidden region in the quantum-dot structure by applying a locally repulsive potential and demonstrate that this configuration is effective at harnessing spin transport. However, we choose to study this model only for simplicity, and it is not special in the sense that there are many alternative configurations that can be used to control spin transport.

The Hamiltonian of the 2D spin-transport system is

$$\hat{\mathcal{H}} = \frac{\hbar^2}{2m}(\hat{k}_x^2 + \hat{k}_y^2)\sigma_0 + \alpha(\hat{\sigma}_x\hat{k}_y - \hat{\sigma}_y\hat{k}_x), \tag{2}$$

where σ_0 is the 2×2 identity matrix and $\hat{\sigma}_x$ and $\hat{\sigma}_y$ are Pauli matrices. To solve the Schrödinger equation, we discretize the cavity into 3888 lattice cells. We set the energy in the unit of $t_0 = \hbar^2/2ma^2$, where a is the lattice constant, and fix the strength of spin-orbit coupling to be $t_{so} = \alpha/2a = 0.1t_0$. Consider an electron entering the quantum-dot system from the left lead. We denote the state in the lead as $|n\rangle$ and, to be specific, we assume that the electron is in the spin-up state. With respect to the dot region, the incoming and outgoing states, respectively, can be written as [49–51]

$$|\text{in}\rangle = |n\rangle \otimes |\sigma = \uparrow\rangle, \tag{3}$$

$$|\text{out}\rangle = \sum_{n',\sigma'} t_{n'n,\sigma'\uparrow}\,|n'\rangle \otimes |\sigma'\rangle, \tag{4}$$

where $t_{n'n,\sigma'\uparrow}$ is the transition amplitude from the incoming state $|n\rangle$ with spin up to the outgoing state $|n'\rangle$ with spin σ. The spin density matrix $\hat{\rho}_s$ carries complete information about the spin state over the orbital degrees of freedom. Let $\hat{\rho}$ be the density matrix characterizing the full state of the system. We can write [50,51] $\hat{\rho}_s = \text{Tr}_{\text{orbit}}[\hat{\rho}]$, which can be expressed in terms of the spin polarization vector defined as the quantum average of the Pauli-spin-operator vector [49–51]:

$$\mathbf{P} = \langle\psi|\hat{\boldsymbol{\sigma}}|\psi\rangle, \tag{5}$$

which contains the information about spin-orbit entanglement or spin decoherence [50,52,53]. The spin density matrix can then be written as [50,51,54]

$$\begin{aligned}\hat{\rho}_s &= \frac{1}{\sum_\sigma \text{Tr}(\boldsymbol{t}_{\sigma\uparrow}\boldsymbol{t}_{\sigma\uparrow}^\dagger)}\begin{pmatrix} \text{Tr}(\boldsymbol{t}_{\uparrow\uparrow}\boldsymbol{t}_{\uparrow\uparrow}^\dagger) & \text{Tr}(\boldsymbol{t}_{\downarrow\uparrow}\boldsymbol{t}_{\uparrow\uparrow}^\dagger) \\ \text{Tr}(\boldsymbol{t}_{\uparrow\uparrow}\boldsymbol{t}_{\downarrow\uparrow}^\dagger) & \text{Tr}(\boldsymbol{t}_{\downarrow\uparrow}\boldsymbol{t}_{\downarrow\uparrow}^\dagger)\end{pmatrix} \\ &= \frac{1}{2}\begin{pmatrix} 1+P_z & P_x - iP_y \\ P_x + iP_y & 1-P_z\end{pmatrix},\end{aligned} \tag{6}$$

where $\boldsymbol{t}_{\sigma\uparrow}$ ($\sigma = \uparrow, \downarrow$) is the spin-resolved transmission matrix for incoming electrons with spin up and outgoing electrons with spin σ. The three components of the polarization vector $\mathbf{P}$ are [18,51]

$$\begin{aligned} P_x &= \frac{2\,\text{Re}\,\text{Tr}(\boldsymbol{t}_{\downarrow\uparrow}\boldsymbol{t}_{\uparrow\uparrow}^\dagger)}{\text{Tr}(\boldsymbol{t}_{\uparrow\uparrow}\boldsymbol{t}_{\uparrow\uparrow}^\dagger) + \text{Tr}(\boldsymbol{t}_{\downarrow\uparrow}\boldsymbol{t}_{\downarrow\uparrow}^\dagger)}, \\ P_y &= \frac{2\,\text{Im}\,\text{Tr}(\boldsymbol{t}_{\downarrow\uparrow}\boldsymbol{t}_{\uparrow\uparrow}^\dagger)}{\text{Tr}(\boldsymbol{t}_{\uparrow\uparrow}\boldsymbol{t}_{\uparrow\uparrow}^\dagger) + \text{Tr}(\boldsymbol{t}_{\downarrow\uparrow}\boldsymbol{t}_{\downarrow\uparrow}^\dagger)}, \\ P_z &= \frac{\text{Tr}(\boldsymbol{t}_{\uparrow\uparrow}\boldsymbol{t}_{\uparrow\uparrow}^\dagger) - \text{Tr}(\boldsymbol{t}_{\downarrow\uparrow}\boldsymbol{t}_{\downarrow\uparrow}^\dagger)}{\text{Tr}(\boldsymbol{t}_{\uparrow\uparrow}\boldsymbol{t}_{\uparrow\uparrow}^\dagger) + \text{Tr}(\boldsymbol{t}_{\downarrow\uparrow}\boldsymbol{t}_{\downarrow\uparrow}^\dagger)}. \end{aligned} \tag{7}$$

Equation (7) indicates that the polarization vector can be expressed solely in terms of the spin-resolved matrix governing the transmission properties. Figure 2 shows the spin-resolved transmission and spin polarization vector versus the Fermi energy. An example of Fano resonance in spin-resolved transmission is shown in Fig. 3. Several examples of Fano resonance in the spin polarization vector are shown in Fig. 4.

In the following, we show analytically that the spin-resolved transmission and the spin polarization vector $\mathbf{P}$ possess Fano resonances characterizable by a formula similar to Eq. (1) for electronic conductance.

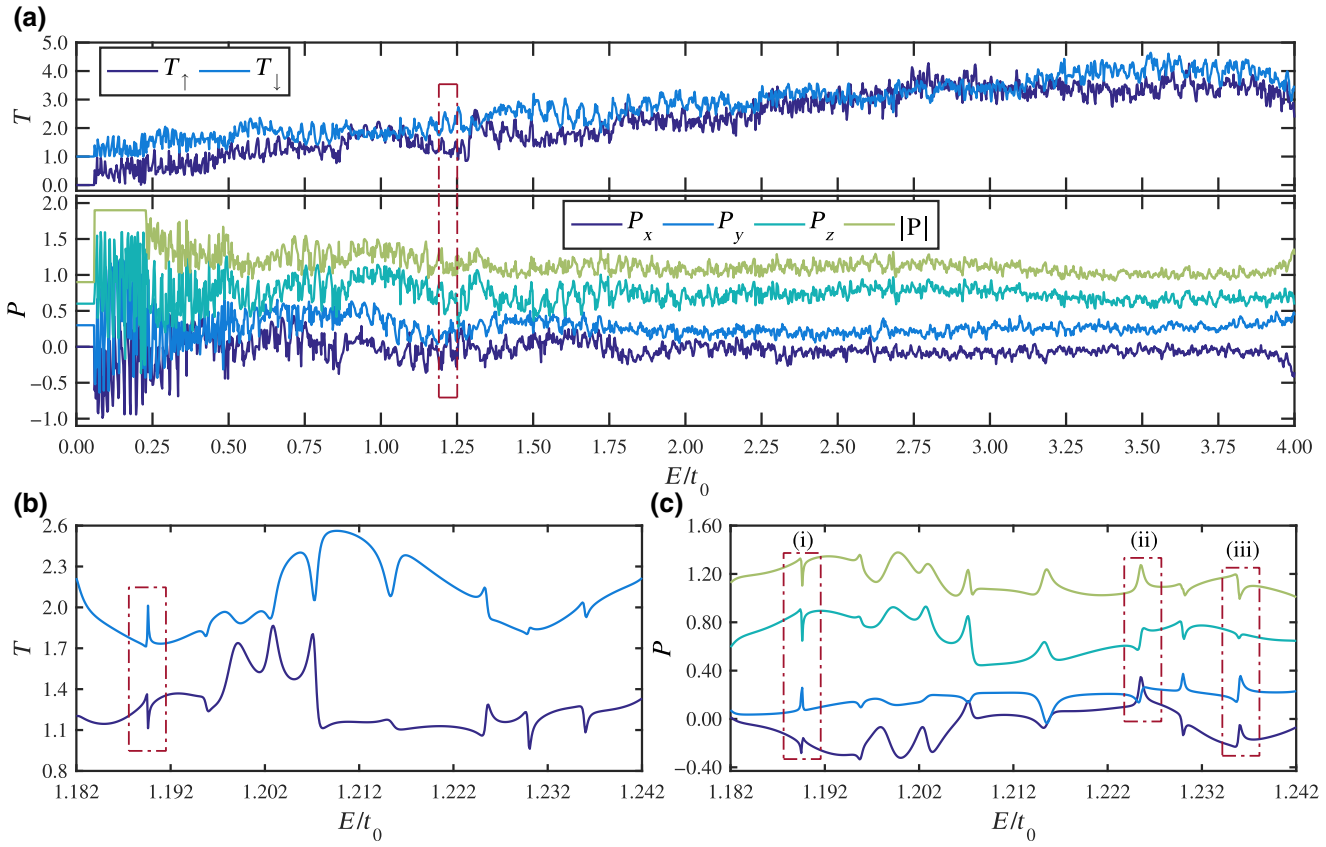

FIG. 2. Spin-resolved transmission and spin polarization vector versus Fermi energy. (a) Variations of the spin-resolved transmission T_σ and the spin polarization vector **P** versus E (in the unit of the hopping energy t_0) in the entire energy interval considered. (b),(c) Enlargement of the behavior of T_σ and the three components of **P** as well as its magnitude, respectively, in an arbitrarily chosen energy interval enclosed by the dash-dotted box in (a). The dash-dotted box covering a resonance peak in (b) is fitted by the theoretical prediction in Fig. 3. The other three dash-dotted boxes labeled as (i), (ii), and (iii) covering three peaks in (c) are fitted by the theoretical results in Fig. 4. The curves from bottom up in (b) correspond to $T_\uparrow$ and $T_\downarrow$, while those in (c) are for P_x, P_y, P_z, and $|\mathbf{P}|$. For visualization, a vertical shift of 1.0 has been applied for $T_\downarrow$ and vertical shifts of 0.3, 0.6, and 0.9 have been applied for P_y, P_z, and $|\mathbf{P}|$, respectively.

III. FANO RESONANCES IN SPIN TRANSPORT AND THE FANO FORMULA

A. Green's function

For 2D mesoscopic electronic transport systems, there have been studies of Fano resonances [2,3,5–7] based on the Green's function, where the spin degree of freedom was ignored. Here we generalize the approach involving the Green's function to spin-transport systems with Rashba spin-orbit interaction.

1. Spin-resolved Green's function

For a typical 2D transport system, the Hamiltonian (2) can be decomposed into two parts: $\hat{H}_c = \hat{H}_o + \hat{H}_{\rm so}$, where $\hat{H}_o$ is the original spinless Hamiltonian, while $\hat{H}_{\rm so}$ is the Hamiltonian for the spin-orbit interaction. The spin-resolved self-energy in the leads can be expressed as $\Sigma^R = \Sigma_0^R \sigma_0$ under the assumption that the self-energies of the spin-up and spin-down states are equal. The effective Hamiltonian of the whole system, taking into account the lead self-energies, can be written as $\hat{H}_s = \hat{H}_c + \Sigma^R$. The Hamiltonian preserves the time-reversal symmetry because the time-reversal operator [55] $\hat{\Theta}$ of the single-particle spin-1/2 system commutes with the Hamiltonian: $[\hat{\Theta}, \hat{H}_s] = 0$. The time-reversal symmetry leads to *Kramers degeneracy*: if state $|n\rangle$ is an eigenstate of the system $\hat{H}$, then its time-reversed state $|\hat{\Theta}n\rangle$ is also an eigenstate with the same energy, where $\langle n|\hat{\Theta}n\rangle = 0$ implying a two-fold degenerate state $|n\rangle$ [54,55].

Because of the inclusion of the self-energies, the system described by the Hamiltonian $\hat{H}_s$ is non-Hermitian with complex eigenvalues and nonidentical left and right eigenstates. The eigenequations distinguishing the left and right eigenstates are

$$\hat{H}_s|\psi_{\alpha,\mu}\rangle = \varepsilon_\alpha|\psi_{\alpha,\mu}\rangle, \tag{8}$$

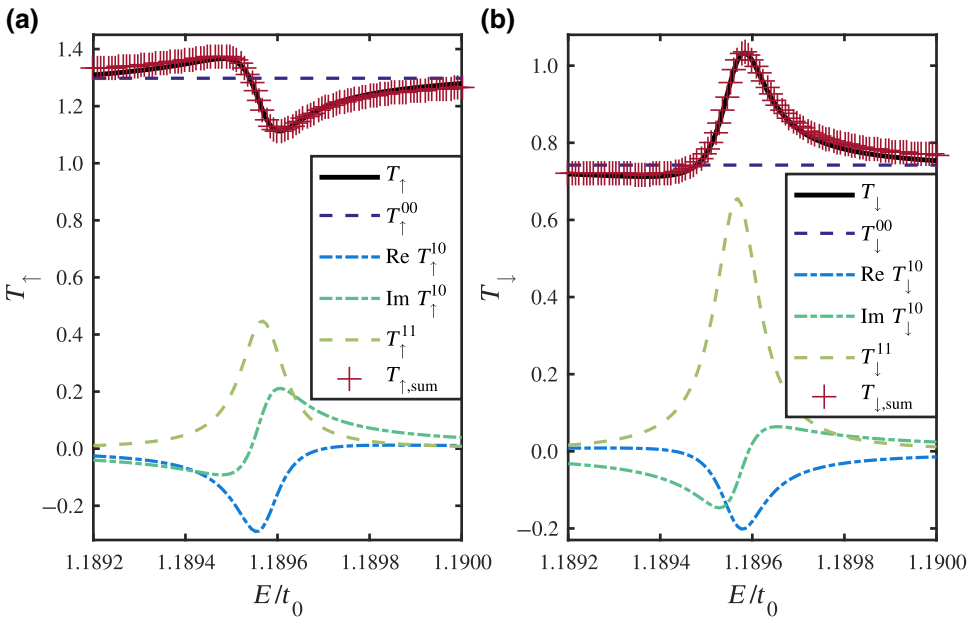

FIG. 3. A Fano resonance in spin-resolved transmission. Comparison of (a) $T_\uparrow$ and (b) $T_\downarrow$ for the peak covered by the dash-dotted box in Fig. 2(b) with Eq. (26). The dark-red pluses are the theoretical prediction and the black curves (mostly beneath the dark-red pluses) represent numerical results.

$$\langle\varphi_{\alpha,\mu}|\hat{H}_s = \langle\varphi_{\alpha,\mu}|\varepsilon_\alpha. \tag{9}$$

where $\mu = 1, 2$ denotes the two Kramer's degenerate eigenstates. The eigenstates $|\psi_{\alpha,\mu}\rangle$ and $|\varphi_{\alpha,\mu}\rangle$ constitute a biorthonormal basis set [4] under the renormalization

$$|\Phi_{\alpha,\mu}\rangle = |\varphi_{\alpha,\mu}\rangle/\langle\varphi_{\alpha,\mu}|\psi_{\beta,\nu}\rangle.$$

The biorthonormal conditions are

$$\langle\Phi_{\alpha,\mu}|\psi_{\beta,\nu}\rangle = \langle\psi_{\alpha,\mu}|\Phi_{\beta,\nu}\rangle = \delta_{\alpha\beta}\delta_{\mu\nu}, \tag{10}$$

with the completeness relation of the eigenwavefunctions

$$\sum_\mu\sum_\alpha |\psi_{\alpha,\mu}\rangle\langle\Phi_{\alpha,\mu}| = \sum_\mu\sum_\alpha |\Phi_{\alpha,\mu}\rangle\langle\psi_{\alpha,\mu}| = 1. \tag{11}$$

For an isolated dot system without any self-energy, the Hamiltonian is Hermitian. In this case, we have

$$\hat{H}_c|\psi_{\alpha,\mu}\rangle = \varepsilon_{\alpha,0}|\psi_{\alpha,\mu}\rangle, \tag{12}$$

with the orthonormal condition

$$\langle\psi_{\alpha,\mu}|\psi_{\beta,\nu}\rangle = \delta_{\alpha\beta}\delta_{\mu\nu}. \tag{13}$$

Using Eqs. (10) and (11), we can derive the Green's function for the central dot region as

$$\begin{aligned} G^R(\mathbf{r},\mathbf{r}') &= \langle\mathbf{r}|\frac{1}{E-\hat{H}_s}|\mathbf{r}'\rangle \\ &= \sum_{\alpha,\mu}\sum_{\beta,\nu}\langle\mathbf{r}|\psi_{\alpha,\mu}\rangle\langle\Phi_{\alpha,\mu}|\frac{1}{E-\hat{H}_s}|\psi_{\beta,\nu}\rangle\langle\Phi_{\beta,\nu}|\mathbf{r}'\rangle \\ &= \sum_{\alpha,\mu}\sum_{\beta,\nu}\psi_{\alpha,\mu}(\mathbf{r})\frac{1}{E-\varepsilon_\beta}\delta_{\alpha\beta}\delta_{\mu\nu}\Phi^\dagger_{\beta,\nu}(\mathbf{r}') \\ &= \sum_\mu\sum_\alpha \frac{\psi_{\alpha,\mu}(\mathbf{r})\Phi^\dagger_{\alpha,\mu}(\mathbf{r}')}{E-\varepsilon_\alpha} \\ &= \begin{pmatrix} G^R_{\uparrow\uparrow}(\mathbf{r},\mathbf{r}') & G^R_{\uparrow\downarrow}(\mathbf{r},\mathbf{r}') \\ G^R_{\downarrow\uparrow}(\mathbf{r},\mathbf{r}') & G^R_{\downarrow\downarrow}(\mathbf{r},\mathbf{r}') \end{pmatrix}. \end{aligned} \tag{14}$$

The spin-resolved Green's function can be written as

$$G^R_{\sigma\sigma'}(\mathbf{r},\mathbf{r}') = \sum_{\mu=1,2}\sum_\alpha \frac{\psi^\sigma_{\alpha,\mu}(\mathbf{r})\Phi^{\sigma'\dagger}_{\alpha,\mu}(\mathbf{r}')}{E-\varepsilon_\alpha}, \quad \sigma,\sigma' = \uparrow,\downarrow. \tag{15}$$

Because of the spin-orbit interaction, the eigenfunctions are spinors:

$$\Phi_{\alpha,\mu}(\mathbf{r}') = \begin{pmatrix} \Phi^\uparrow_{\alpha,\mu}(\mathbf{r}') \\ \Phi^\downarrow_{\alpha,\mu}(\mathbf{r}') \end{pmatrix},$$

$$\psi_{\alpha,\mu}(\mathbf{r}) = \begin{pmatrix} \psi^\uparrow_{\alpha,\mu}(\mathbf{r}) \\ \psi^\downarrow_{\alpha,\mu}(\mathbf{r}) \end{pmatrix}.$$

Treating the self-energy Σ^R as a perturbation [4,11], we can use the perturbation theory to expand the eigenenergies

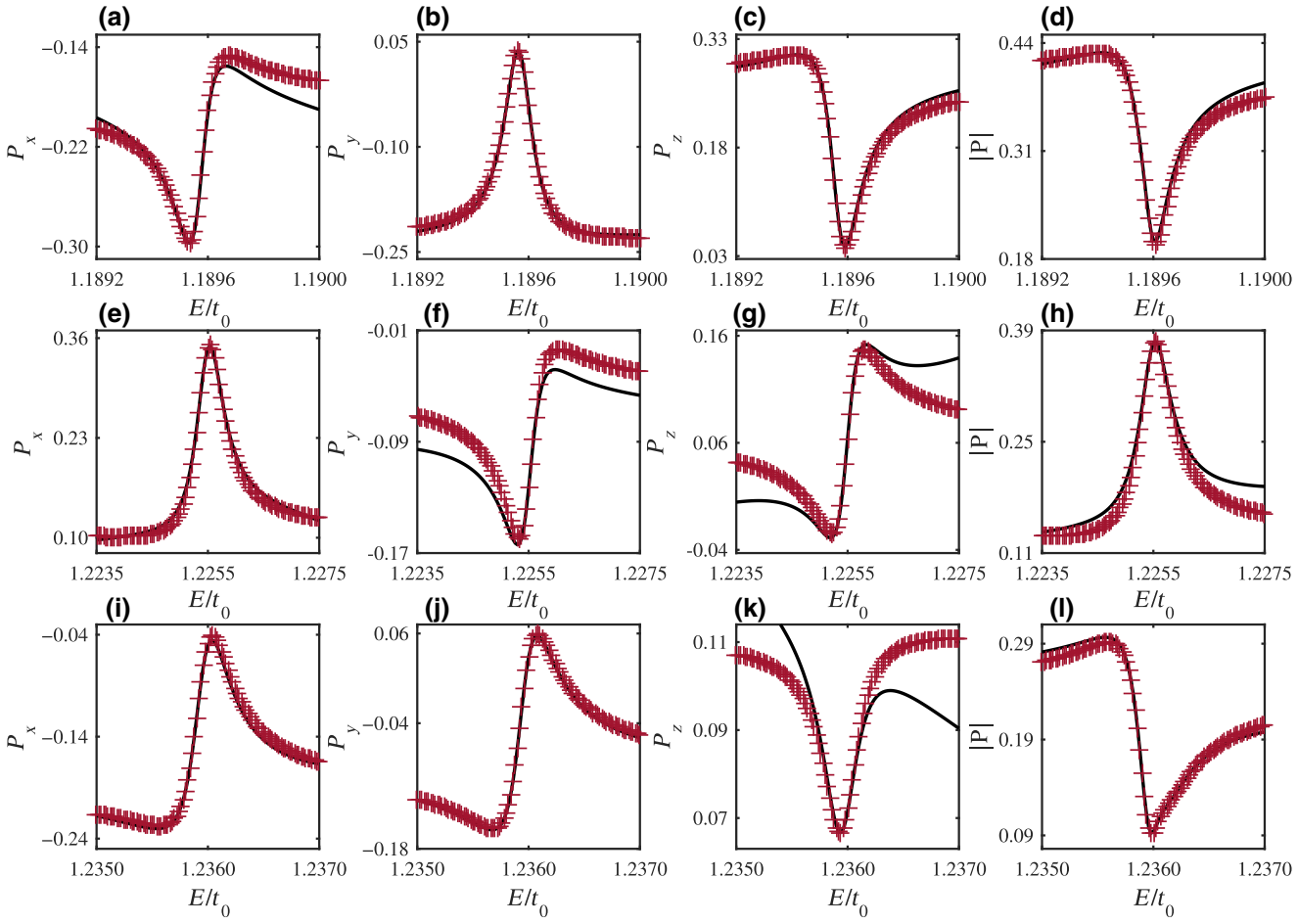

FIG. 4. For the components of the spin polarization vector **P** presented in Eq. (29), the three rows correspond to the three peaks covered by the dash-dotted boxes labeled as (i), (ii), and (iii), respectively, in Fig. 2(c), and the four columns show the numerical (black curve) and theoretical (plus symbols) results for P_x, P_y, P_z, and $|\mathbf{P}|$, respectively.

and the eigenstates as

$$\varepsilon_\alpha = \varepsilon_{0,\alpha} - \delta_\alpha - i\gamma_\alpha, \tag{16}$$

$$|\psi_{\alpha,\mu}\rangle = |\psi_{0\alpha,\mu}\rangle - |\psi_{r\alpha,\mu}\rangle - i|\psi_{i\alpha,\mu}\rangle. \tag{17}$$

Substituting Eqs. (16) and (17) into Eq. (9), we get

$$\begin{aligned}&(\hat{H}_c + \Sigma^R)(|\psi_{0\alpha,\mu}\rangle - |\psi_{r\alpha,\mu}\rangle - i|\psi_{i\alpha,\mu}\rangle)\\ &\quad = (\varepsilon_{0,\alpha} - \delta_\alpha - i\gamma_\alpha)(|\psi_{0\alpha,\mu}\rangle - |\psi_{r\alpha,\mu}\rangle - i|\psi_{i\alpha,\mu}\rangle).\end{aligned}$$

Substituting Eq. (12) into the above equation, ignoring second-order terms on both sides, and left-multiplying both sides by $\langle\psi_{0\alpha,\mu}|$, we obtain [4,11]

$$\begin{aligned}\delta_\alpha + i\gamma_\alpha &\simeq -\sum_\mu \langle\psi_{0\alpha,\mu}|\Sigma^R|\psi_{0\alpha,\mu}\rangle\\ &= -\sum_{\mu,\sigma}\langle\psi^\sigma_{0\alpha,\mu}|\Sigma^R_0|\psi^\sigma_{0\alpha,\mu}\rangle,\end{aligned} \tag{18}$$

where the spin components of the eigenstates and the relation $\Sigma^R = \Sigma^R_0\sigma_0$ have been used. Equation (16) can be rewritten as

$$\varepsilon_\alpha \simeq \varepsilon_{\alpha,0} - \sum_{\mu,\sigma}\langle\psi^\sigma_{0\alpha,\mu}|\Sigma^R_0|\psi^\sigma_{0\alpha,\mu}\rangle. \tag{19}$$

The resonance width γ_α can be obtained from Eq. (18) as [4,11]

$$\begin{aligned}\gamma_\alpha &= -\mathrm{Im}\left(\sum_{\mu,\sigma}\langle\psi^\sigma_{0\alpha,\mu}|\Sigma^R_0|\psi^\sigma_{0\alpha,\mu}\rangle\right)\\ &= \sum_{\mu,\sigma}\langle\psi^\sigma_{0\alpha,\mu}| - \mathrm{Im}\,\Sigma^R_0|\psi^\sigma_{0\alpha,\mu}\rangle.\end{aligned} \tag{20}$$

This expression is validated by comparing it with the exact value in Eq. (16); see Fig. 5.

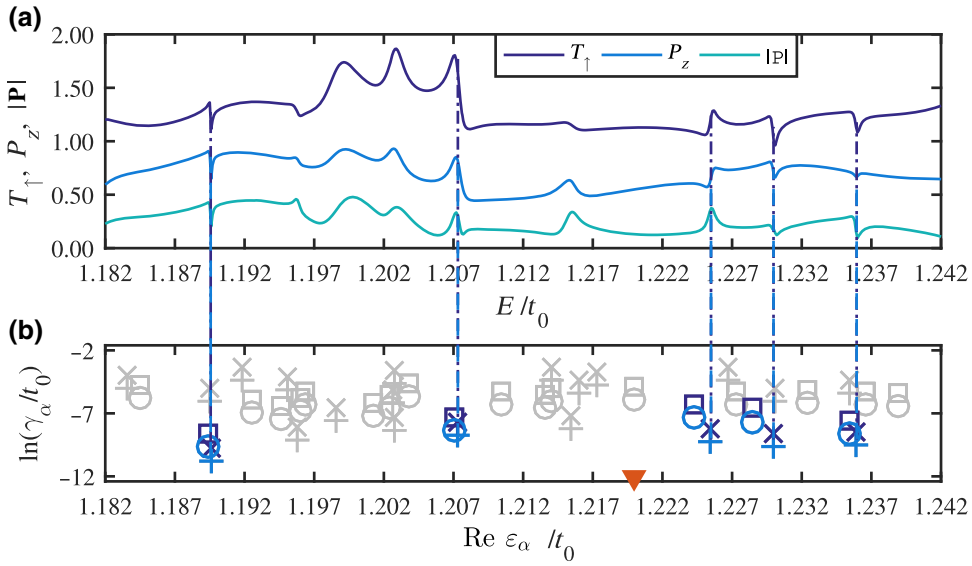

FIG. 5. Comparison of Fano-resonance widths obtained numerically and theoreically for spin-resolved transmission and the spin polarization vector. (a) Spin-resolved transmission $T_\uparrow$ and the z component and the magnitude of the polarization vector, P_z and $|\mathbf{P}|$, respectively, versus E in the unit of t_0. (b) $\ln(\gamma_\alpha/t_0)$ for $T_\uparrow$ and P_z or $|\mathbf{P}|$ versus $\mathrm{Re}\,\varepsilon_\alpha$. The symbols $\times$ and $\square$ denote $\ln(\gamma_\alpha/t_0)$ from Eqs. (16) and (20), respectively, for $T_\uparrow$. The symbols **+** and $\bigcirc$ represent $\ln(\gamma_\alpha/t_0)$ in Eqs. (16) and (20), respectively, both being corrected by Eq. (32) for P_z or $|\mathbf{P}|$. The point $E_0 = 1.22t_0$ is marked as a red triangle on the horizontal axis of (b). For visualization purposes, the curve of P_z has been shifted up by 0.6, while the others are unshifted.

2. Fisher-Lee relation

The Fisher-Lee relation connects the S matrix with the Green's function [4,24]. For a two-terminal system with left and right leads, the spin-resolved Fisher-Lee relation can be expressed as

$$\begin{aligned} s^{\sigma\sigma'}_{nm} &= -\delta_{mn}\delta^{\sigma\sigma'} + i\hbar\sqrt{v_m v_n}\int \chi_n(y_q)G^R_{\sigma\sigma'}\chi_m(y_p)dy_p dy_q \\ &= -\delta_{mn}\delta^{\sigma\sigma'} + i\sqrt{\hbar v_n}\times R^{\sigma\sigma'}_{nm}\times\sqrt{\hbar v_m}, \end{aligned} \tag{21}$$

where m and n belong to lead p and lead q, respectively, and

$$\begin{aligned} R^{\sigma\sigma'}_{nm} &= \sum_{\mu=1,2}\sum_{\alpha}\frac{\psi^{\sigma}_{\alpha n,\mu}(x_q)\Phi^{\sigma'\dagger}_{\alpha m,\mu}(x_p)}{E-\varepsilon_\alpha}, \\ \psi^{\sigma}_{\alpha n,\mu}(x_q) &= \int \chi_n(y_q)\psi^{\sigma}_{\alpha n,\mu}(x_q,y_q)dy_q, \\ \Phi^{\sigma'}_{\alpha m,\mu}(x_p) &= \int \chi_m(y_p)\Phi^{\sigma'}_{\alpha m,\mu}(x_p,y_p)dy_p, \\ V_{p/q} &= \mathrm{diag}\{\hbar v_1,\hbar v_2,\ldots,\hbar v_{N_{p/q}}\}. \end{aligned}$$

For $p\neq q$, $s^{\sigma\sigma'}_{nm}$ gives the spin resolved transmission matrix, while for $p=q$, it is the reflection matrix. The spin-resolved transmission matrix can be expressed in the following concise form:

$$t_{\sigma\sigma'} = i\sqrt{V_q}\times R^{\sigma\sigma'}\times\sqrt{V_p}. \tag{22}$$

For convenience, we let p and q specify the left lead and the right lead, respectively. With the spin-resolved transmission matrix, we can calculate the spin-resolved transmission and the spin polarization vector in Eq. (7).

B. Fano resonances in spin-resolved transmission and the spin polarization vector

We derive Fano-resonance formulas for spin-resolved transmission and the spin polarization vector **P**. Say we select E_0 as the energy of interest. If E_0 approaches an eigenenergy of the closed dot system, a pole will arise in $R_{\sigma\sigma',nm}$, corresponding to a specific state labeled by, for example, α. We can then separate state α from the sum in $R_{\sigma\sigma',nm}$ to get two terms: one term slowly varying (with energy) and the other term rapidly changing, where the former acts effectively as the background, while the latter varies rapidly in the small energy interval containing state α [11,20,22,24]. Specifically, we have

$$\begin{aligned} R^{\sigma\sigma'}_{nm} = R^{0,\sigma\sigma'}_{nm} + R^{1,\sigma\sigma'}_{nm} &= \sum_{\mu=1,2}\sum_{\beta\neq\alpha}\frac{\psi^{\sigma}_{\beta n,\mu}(x_r)\Phi^{\sigma'\dagger}_{\beta m,\mu}(x_l)}{E-\varepsilon_\beta} \\ &+ \sum_{\mu=1,2}\frac{\psi^{\sigma}_{\alpha n,\mu}(x_r)\Phi^{\sigma'\dagger}_{\alpha m,\mu}(x_l)}{E-\varepsilon_\alpha}. \end{aligned} \tag{23}$$

The spin-resolved transmission matrix in Eq. (22) can be rewritten as the sum of the slowly varying background term and the fast-changing resonance term. For the incoming spin-up state, we have

$$\boldsymbol{t}_{\sigma\uparrow} = \boldsymbol{t}^0_{\sigma\uparrow} + \boldsymbol{t}^1_{\sigma\uparrow}, \tag{24}$$

where the first and second terms represent the slow and fast terms, respectively. The spin-resolved transmission

$$T_\sigma = \mathrm{Tr}(\boldsymbol{t}_{\sigma\uparrow}\boldsymbol{t}^\dagger_{\sigma\uparrow})$$

can be obtained, from which the Fano-resonance formulas for T_σ and $\mathbf{P}$ can be derived.

1. Fano formula for spin-resolved transmission T_σ

Substituting Eq. (24) into the definition of the spin-resolved transmission T_σ, we have

$$\begin{aligned} T_\sigma &= \mathrm{Tr}(\boldsymbol{t}_{\sigma\uparrow}\boldsymbol{t}^\dagger_{\sigma\uparrow}) \\ &= \mathrm{Tr}[(\boldsymbol{t}^0_{\sigma\uparrow} + \boldsymbol{t}^1_{\sigma\uparrow})(\boldsymbol{t}^0_{\sigma\uparrow} + \boldsymbol{t}^1_{\sigma\uparrow})^\dagger] \\ &= \mathrm{Tr}(\boldsymbol{t}^0_{\sigma\uparrow}\boldsymbol{t}^{0\dagger}_{\sigma\uparrow}) + \mathrm{Tr}(\boldsymbol{t}^0_{\sigma\uparrow}\boldsymbol{t}^{1\dagger}_{\sigma\uparrow}) + \mathrm{Tr}(\boldsymbol{t}^1_{\sigma\uparrow}\boldsymbol{t}^{0\dagger}_{\sigma\uparrow}) + \mathrm{Tr}(\boldsymbol{t}^1_{\sigma\uparrow}\boldsymbol{t}^{1\dagger}_{\sigma\uparrow}) \\ &= T^{00}_\sigma + T^{01}_\sigma + T^{10}_\sigma + T^{11}_\sigma, \end{aligned}$$

where $T^{00}_\sigma(E) \simeq T^{00}_\sigma(E_0)$ is approximately a constant [11] in the small energy interval containing the specific energy value E_α. Letting $\epsilon \equiv (E - E_\alpha)/\gamma_\alpha$ and $\epsilon_0 \equiv (E_0 - E_\alpha)/\gamma_\alpha$, we have

$$\begin{aligned} T^{01}_\sigma(E) &= T^{01}_\sigma(E_0)\frac{E_0 - E_\alpha - i\gamma_\alpha}{E - E_\alpha - i\gamma_\alpha} \\ &= T^{01}_\sigma(E_0)\frac{\epsilon_0 - i}{\epsilon - i}, \\ T^{10}_\sigma(E) &= T^{10}_\sigma(E_0)\frac{E_0 - E_\alpha + i\gamma_\alpha}{E - E_\alpha + i\gamma_\alpha} \\ &= T^{10}_\sigma(E_0)\frac{\epsilon_0 + i}{\epsilon + i}, \\ T^{11}_\sigma(E) &= T^{11}_\sigma(E_0)\frac{(E_0 - E_\alpha)^2 + \gamma^2_\alpha}{(E - E_\alpha)^2 + \gamma^2_\alpha} \\ &= T^{11}_\sigma(E_0)\frac{\epsilon^2_0 + 1}{\epsilon^2 + 1}. \end{aligned}$$

For $E_0 = E_\alpha$, we have $\epsilon_0 = 0$. Denoting

$$\Delta T_\sigma = T^{01}_\sigma(E_0) + T^{10}_\sigma(E_0) + T^{11}_\sigma(E_0), \tag{25a}$$

$$q_\sigma = \frac{i}{2}\frac{T^{10}_\sigma(E_0) - T^{01}_\sigma(E_0)}{\Delta T_\sigma(E_0)}, \tag{25b}$$

we obtain an explicit expression for $T_{\sigma,\mathrm{sum}}$:

$$\begin{aligned} T_{\sigma,\mathrm{sum}} &= T^{00}_\sigma + T^{01}_\sigma + T^{10}_\sigma + T^{11}_\sigma \\ &= T^{00}_\sigma + \frac{1 + 2q_\sigma\epsilon}{1 + \epsilon^2}\Delta T_\sigma \\ &= |t^{\mathrm{bg}}_\sigma|^2\frac{|\epsilon + q'_\sigma|^2}{\epsilon^2 + 1}, \end{aligned} \tag{26}$$

with the relation

$$\begin{aligned} |t^{\mathrm{bg}}_\sigma|^2 &= T^{00}_\sigma, \\ \mathrm{Re}\, q'_\sigma &= \Delta T_\sigma q_\sigma / T^{00}_\sigma, \\ \mathrm{Im}\, q'_\sigma &= \sqrt{1 + \Delta T_\sigma/T^{00}_\sigma - q^2_\sigma(\Delta T_\sigma/T^{00}_\sigma)^2}. \end{aligned}$$

Equation (26) presents the Fano-resonance form [11,20] with the complex profile parameter q'_σ that depends on q_σ, T^{00}_σ, and ΔT_σ. Fano resonances in the spin-resolved transmission can thus be characterized by a formula similar in form to that for the spinless conductance in Refs. [11,24].

2. Fano-resonance formula for the spin polarization vector

The components of $\mathbf{P}$ in Eq. (7) depend on T_σ and the cross term of the spin density matrix denoted as

$$T_c = \mathrm{Tr}(\boldsymbol{t}_{\downarrow\uparrow}\boldsymbol{t}^\dagger_{\uparrow\uparrow}).$$

We check and find that T_c exhibits Fano resonances that can be described by the same formula as for T_σ. Particularly, we have

$$\begin{aligned} T_{c,\mathrm{sum}} &= T^{00}_c + T^{01}_c + T^{10}_c + T^{11}_c \\ &= T^{00}_c + \frac{1 + 2q_c\epsilon}{1 + \epsilon^2}\Delta T_c \\ &= |t^{\mathrm{bg}}_c|^2\frac{|\epsilon + q'_c|^2}{\epsilon^2 + 1}, \end{aligned} \tag{27}$$

where the coefficients are given by

$$\Delta T_c = T^{01}_c(E_0) + T^{10}_c(E_0) + T^{11}_c(E_0), \tag{28a}$$

$$q_c = \frac{i}{2}\frac{T^{10}_c(E_0) - T^{01}_c(E_0)}{\Delta T_c(E_0)}, \tag{28b}$$

with the relations

$$\begin{aligned} |t^{\mathrm{bg}}_c|^2 &= T^{00}_c, \\ \mathrm{Re}\, q'_c &= \Delta T_c q_c / T^{00}_c, \\ \mathrm{Im}\, q'_c &= \sqrt{1 + \Delta T_c/T^{00}_c - q^2_c(\Delta T_c/T^{00}_c)^2}. \end{aligned}$$

To obtain a Fano formula for the spin polarization vector, we need to substitute the quantity T_σ in Eq. (26) and the

quantity T_c in Eq. (27) into Eq. (7). Note that the components of **P** are fractions with both the numerator and the denominator expressed by the trace of the spin-resolved transmission matrix. After some algebraic manipulation, we obtain

$$P_i = P_{i,0} + \frac{1+2Q\Xi}{1+\Xi^2}\Delta P_i = |p_i^{\rm bg}|^2 \frac{|Q'+\Xi|^2}{1+\Xi^2}, \tag{29}$$

where $i = x, y, z$ denotes the three components of the spin polarization vector and the renormalized energy is

$$\Xi = \sqrt{S}\left[\epsilon + \frac{\sum_\sigma (q_\sigma \Delta T_\sigma)}{\sum_\sigma T_\sigma^{00}}\right] = \frac{E - \left[\mathrm{Re}\,\varepsilon_\alpha - \gamma_\alpha \frac{\sum_\sigma (q_\sigma \Delta T_\sigma)}{\sum_\sigma T_\sigma^{00}}\right]}{\gamma_\alpha/\sqrt{S}}. \tag{30}$$

With the coefficients in Eq. (29), we can combine Eqs. (25a) and (28a) to get

$$P_0 = \frac{\hat{\mathrm{O}} T_s^{00}}{\sum_\sigma T_\sigma^{00}},$$

$$\Delta P = \frac{\hat{\mathrm{O}}\Delta T_s - P_0 \sum_\sigma \Delta T_\sigma - 2[\hat{\mathrm{O}}(q_s \Delta T_s) - P_0 \sum_\sigma (q_\sigma \Delta T_\sigma)] \frac{\sum_\sigma (q_\sigma \Delta T_\sigma)}{\sum_\sigma T_\sigma^{00}}}{(\sum_\sigma T_\sigma^{00} + \sum_\sigma \Delta T_\sigma) - \frac{[\sum_\sigma (q_\sigma \Delta T_\sigma)]^2}{\sum_\sigma T_\sigma^{00}}},$$

$$Q = \frac{1}{\sqrt{S}} \frac{\hat{\mathrm{O}}(q_s \Delta T_s) - P_0 \sum_\sigma (q_\sigma \Delta T_\sigma)}{\hat{\mathrm{O}}\Delta T_s - P_0 \sum_\sigma \Delta T_\sigma - 2[\hat{\mathrm{O}}(q_s \Delta T_s) - P_0 \sum_\sigma (q_\sigma \Delta T_\sigma)] \frac{\sum_\sigma (q_\sigma \Delta T_\sigma)}{\sum_\sigma T_\sigma^{00}}},$$

$$S = \frac{\sum_\sigma T_\sigma^{00}}{(\sum_\sigma T_\sigma^{00} + \sum_\sigma \Delta T_\sigma) - \frac{[\sum_\sigma (q_\sigma \Delta T_\sigma)]^2}{\sum_\sigma T_\sigma^{00}}},$$

where $\hat{\mathrm{O}}$ is an operator acting as, for example, for T_s and $s = \{c, \sigma\}$, $\hat{\mathrm{O}} T_s = \{2\mathrm{Re}\, T_c, 2\mathrm{Im}\, T_c, \ominus T_\sigma\}$, where $\ominus T_\sigma = T_\uparrow - T_\downarrow$. The three components correspond to $\{P_x, P_y, P_z\}$, respectively. The relations among the quantities p_i^{bg}, Q', $P_{i,0}$, ΔP_i, and Q are

$$|p_i^{bg}|^2 = P_{i,0},$$
$$\mathrm{Re}\, Q' = \Delta P_i Q / P_{i,0},$$
$$\mathrm{Im}\, Q' = \sqrt{1 + \Delta P_i/P_{i,0} - Q^2 (\Delta P_i/P_{i,0})^2},$$

where the parameter Q' governs the shape of the Fano-resonance profile [1,2,11,20]. In addition, Eq. (30) gives corrections for the peak position and for the width for the spin polarization vector [Eq. (29)] in comparison with those in T_σ and T_c. In particular, the new position and width are, respectively,

$$E'_\alpha = \mathrm{Re}\,\varepsilon_\alpha - \gamma_\alpha \frac{\sum_\sigma (q_\sigma \Delta T_\sigma)}{\sum_\sigma T_\sigma^{00}}, \tag{31}$$

$$\gamma'_\alpha = \gamma_\alpha/\sqrt{S}. \tag{32}$$

These corrections are typically insignificant. To demonstrate this point, we compare [56,57] the peak positions and widths of various resonances by plotting the logarithm of the width, $\ln \gamma_\alpha$, versus $\mathrm{Re}\,\epsilon_\alpha$ for $T_\uparrow$, P_z, and $|\mathbf{P}|$ as shown in Fig. 5. There are five resonance peaks, whose numerically obtained locations from Eq. (16) (marked by a cross) can be compared with the theoretical predictions (marked by a square) from Eq. (20). For the same resonance peaks of **P**, the corrected results from Eq. (32) for both the numerical [from Eq. (16), marked by a plus sign] and the theoretical [from Eq. (20), marked by a circle] values are also included. It can be seen that the three types of results agree well with each other. Overall, these results provide strong evidence that both the spin polarization vector **P** and the spin-resolved transmission T_σ follow the Fano-resonance profile.

C. Effect of dot geometry on Fano resonances in spin transmission and polarization

In general, in 2D spin transport, spin-resolved transmission and spin polarization depend on the dot structure [51], and the Fano-resonance peaks arise due to the coupling between the quantum states in the lead and in the

dot region. For example, when the Fermi energy is close to that of a bounded state in the corresponding closed dot region, the interaction between the propagating mode in the lead and the remnant of the bounded states in the open dot region will be strengthened, leading to a Fano-resonance peak [2]. If we modify the geometric structure of the dot region, the original bound state at this energy will in general disappear, so will the Fano resonance. We expect this "washing-out" effect or disappearance of resonances to occur for quantities underlying spin transport, especially spin-resolved transmission and the polarization vector.

To demonstrate the effect of variations in the dot geometry on Fano resonances in spin transmission and polarization, we modify the dot structure by adding a hard circular disk at the center of the dot region. Figure 6 shows representative results. Especially, Fig. 6(a) shows the curves of $T_\uparrow$ (upper panel) and $|\mathbf{P}|$ (lower panel) for two cases: (i) unmodified dot structure of radius $R = 0.6\ \mu$m, cut width $w = 0.7R$, and lead with $h = 0.2R$ ($N = 12$ modes)—the lower blue curves—and (ii) modified dot structure with a central circular region removed (equivalent to a circular hard disk for electron waves and can be realized by applying a local gate potential draining out the electrons)—the upper orange curves. It can be seen that the four Fano resonance peaks labeled 1–4 on the lower blue curves in the energy range are drastically smoothed out by the geometric modification of the dot structure. This effect can be further seen by examining the local density of state defined as [4]

$$\rho(\mathbf{r}; E) = -\frac{1}{\pi}\mathrm{Im}[G^R(\mathbf{r}, \mathbf{r}; E)]. \tag{33}$$

Figures 6(b) shows the local density of state associated with the four Fano-resonance peaks in the unmodified system, which exhibits a strongly localized behavior. For the same energy, the localization no longer exists in the modified dot, signifying the disappearance of the original Fano resonances. A practical implication of the results in Fig. 6 is that spin transport and Fano resonances can be modulated through geometric modifications of the dot structure, which can be experimentally realized by applying a judiciously designed gate potential profile to the quantum dot [56,57].

D. Electronic switch device for spin transport

Spin Fano resonances can be used for device applications. Here we present the design of an electronic switch that can control the spin orientation of the electrons associated with the output current. The basic structure of the device is a semiconductor heterostructure, as shown in Fig. 7(a), where the confining boundary has the shape shown in Fig. 1(a). A gate potential is applied to a circular region above the cavity with a controlling switch. When the switch is *off* , electrons move ballistically inside the cavity, whose classical dynamics are mixed with stable periodic orbits, leading to sharp Fano resonances. When

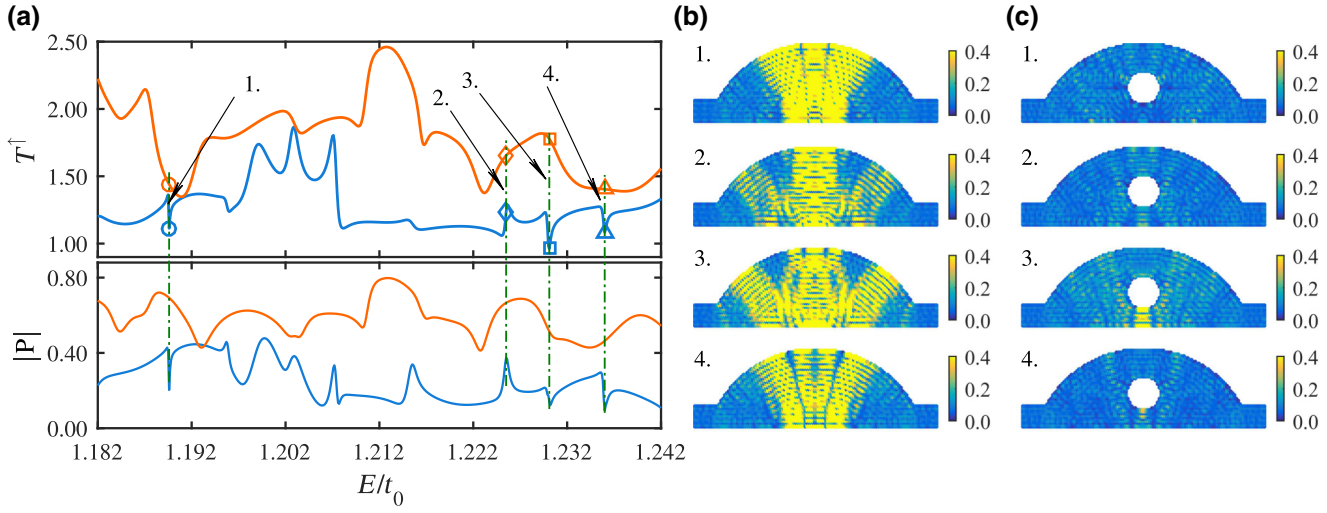

FIG. 6. Shape dependence of spin transport. (a) Spin-resolved transmission $T_\uparrow$ and the magnitude of the spin polarization vector $|\mathbf{P}|$ versus E in the unit of t_0 for a bow-shaped dot region (the lower curves). There are four peaks with their corresponding energies marked by different symbols labeled as 1–4. The upper curves (shifted upward by 0.3 for both $T_\uparrow$ and $|\mathbf{P}|$) correspond to the same quantities but for a modified geometry of the dot region: there is a hard circle of radius $r = 0.2R$ located at the center of the original bow-shaped dot, into which waves are unable to penetrate. The original sharp Fano resonances have been smoothed out by alteration of the geometric structure of the dot. (b),(c) Two-dimensional maps of the density of states associated with the four peaks in (a) for the original bow-shaped dot and the modified-dot structure with a central circular forbidden region, respectively. Associated with the original sharp resonances are strongly localized states in (b), whereas such states no longer exist for the modified dot.

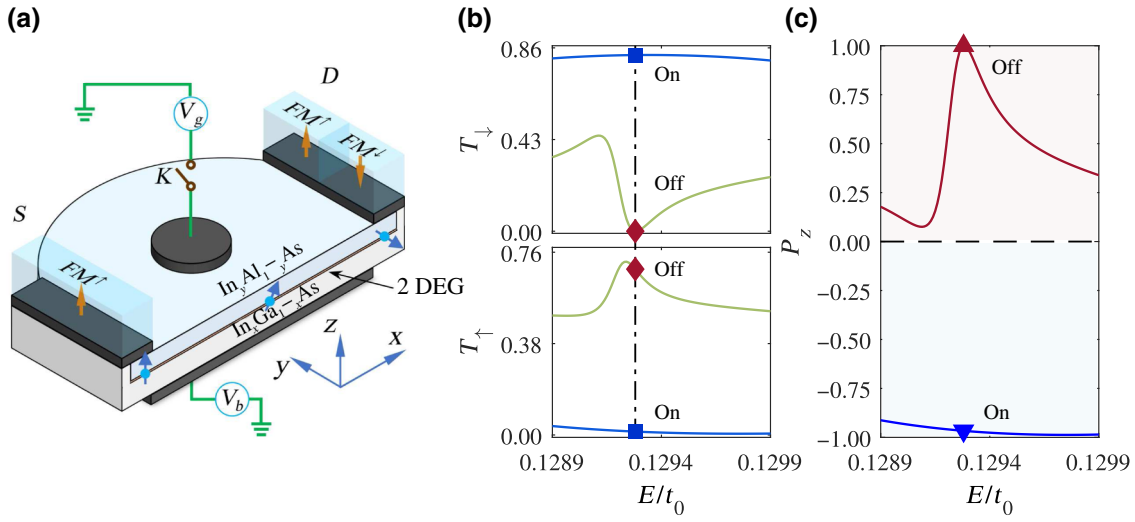

FIG. 7. An electronic switch for spin transport. (a) The proposed electronic switch device using a spin Fano resonance. The device is a semiconductor heterostructure (e.g., $In_xGa_{1-x}As/In_yAl_{1-y}As$) [58]. Terminal S is a ferromagnetic source that emits spin-up-polarized electrons only, while terminal D possesses two independent ferromagnetic drains that are able to detect either spin-up-polarized or spin-down-polarized electrons. The back gate with V_b can be used to produce the Rashba electric field. The circular gate inside the structure with $V_g < 0$ repels electrons, producing an effective circular forbidden region. (b) Spin-dependent transmission $T_{\downarrow}$ and $T_{\uparrow}$ versus E in the unit of t_0 in an interval covering a specific Fano-resonance peak. For each quantity, two cases are plotted with the switch either *on* or *off*. (c) Spin polarization P_z versus E in the same range as in (b), which demonstrates the working of the switch: for $E/t_0 = 0.1293$ as marked by the symbols in (b),(c), when the switch is *on*, $T_{\uparrow}$ is close to zero and $P_z \approx -1$, so the output current is almost purely associated with spin-down electrons. When the switch is *off* , $T_{\downarrow} = 0$ and $P_z = 1$, so the output current consists purely of spin-up electrons. FM, ferromagnet.

the switch is *on* so that a negative potential is applied, the electrons under the circular gate will be repelled out, forming effectively a circular forbidden region, as shown in Fig. 6(c), leading to drastic and characteristic changes in the underlying classical dynamics. As a result, the originally sharp Fano resonances will be either broadened or removed, generating distinct spin-transport behaviors.

To explain the working of the device, we present a concrete example. In particular, we choose the Fermi energy to be $E/t_0 = 0.1293$, which corresponds to a spin Fano resonance. Figures 7(b) and 7(c) demonstrate that the output current can be controlled to either be made up of purely spin-up electrons (when the gate potential is *off*), or consist of almost-purely spin-down electrons (with gate potential *on*). We see that the energy for $T_{\uparrow}$ to reach a maximum and that for $T_{\downarrow}$ to become a minimum are nearly identical, but with a small difference. The reason is that when $T_{\uparrow}$ takes on a maximum value, $T_{\downarrow}$ will no longer be zero but will have a small value, with their sum being 1. Nevertheless, whether the gate voltage is *off* or *on* can cause the electrons constituting the output current to be either spin-up or spin-down electrons, respectively. There are other Fano-resonance peaks at which the gate potential can make the spin of the output electrons either polarized in the z direction, where the value of P_z can be close to 1 or -1, or polarized in the x-y plane, where the value of P_z is close to zero. For different spin Fano resonances, the device can thus generate electrons with drastically different spin orientations.

IV. CONCLUSION AND DISCUSSION

We generalize the universal Fano-resonance formula describing quantities associated with electronic transport in 2D mesoscopic systems (e.g., conductance) to two key quantities underlying spin transport: spin-resolved transmission and the spin polarization vector. The fact that Fano resonances, regardless of the nature of the transport (electronic or spin), are described by formulas of essentially the same form is a strong indication of the same physics underlying the transport or scattering processes: Fano resonances are the result of the interaction between the continuous propagating states in the waveguide leads and the discrete states in the scattering region. While our analysis is of the perturbative type, where the self-energies describing the interactions are treated as a perturbation, the resonance peaks in the spin-resolved transmission and the spin polarization vector predicted by two slightly different theories agree well not only with each other but also with those from direct numerical simulation, validating the analysis. We also demonstrate that Fano resonances in spin transport can be smoothed out or even removed through geometric modifications of the scattering region. There have already been studies of control of quantum transport

with respect to electronic properties [20,22,24,25], especially the scheme using geometric modification to modulate conductance fluctuations [56,57]. Our results suggest that the same principle can be applied to spin transport. Especially, given that the Fermi energy takes on the value for a particular Fano resonance, by changing the nature of the classical dynamics (e.g., through a properly designed local gate potential) we can weaken or enhance the resonance, leading to drastic changes in the spin-transport properties. This effect can be used to design electronically controlled switches for spin transport, a key component in spintronic devices.

We wish to further clarify that our work is motivated by the fact that, while Fano resonances associated with electronic transport are reasonably well understood, a systematic and quantitative understanding of spin Fano resonances is lacking. The goals of our study are to gain such an understanding and to design an electrically controlled switch for spin transport with an eye toward potential applications in spintronics. As explained, our understanding of how spin Fano resonances emerge naturally leads to a mechanism for their breakdown: localized states can be removed by altering the nature of the corresponding classical dynamics, and this has significance in practical applications.

It is generally true that the origin of the Fano resonance lies in the properties of the S matrix, and any observable built from it should exhibit a Fano profile. However, it is is highly nontrivial to derive explicitly the resonance profiles for general physical observables. For example, as demonstrated in previous work [5], even if the channel-to-channel scattering Fano profile is known, it is far from straightforward to obtain the overall resonance profile for the transmission. To derive the resonance profile for spin transport, we follow the standard method of decomposing the Green's function into a slow component and a fast component, but the derivation is much-more challenging and sophisticated than that without spin, making our analytic derivation a meaningful contribution to the field.

Broadly, Fano resonances are a common phenomenon in a large variety of quantum transport and scattering systems. The contribution of our work is that, for spin-resolved transport systems, not only can Fano resonances occur in the total current, but the spin-resolved current and the spin polarization vector can also exhibit such resonances. From a theoretical point of view, we develop a framework to generalize the conventional Green's function formalism to spin transport and use the Fisher-Lee relation to obtain the spin-resolved transmission matrix, from which the spin polarization vector is calculated. Treating the coupling to the leads as a perturbation and separating the Green's function into a slow component and a fast component, we succeed in deriving explicit formulas for spin resonances. Our theory predicts that classical chaos can have a dramatic effect on the width of the spin Fano resonance, which is verified numerically with a generic type of dot geometry that generates nonhyperbolic chaotic dynamics in the classical limit. Use of the classical chaos also leads to a regularization scheme for spin-resolved transmission and spin polarization fluctuations with potential benefits for spintronics. To our knowledge, before our work, explicit formulas for spin Fano resonance did not exist. Furthermore, while there are previous studies on the effect of classical chaos on spin transport [51,59–63], the understanding of how chaos helps remove or weaken spin Fano resonances was at a qualitative level. Our present work provides a quantitative understanding.

ACKNOWLEDGMENTS

This work was supported by the National Natural Science Foundation of China under Grants No. 11775101, No. 11834005, and No. 11674139. Y.C.L. is supported by the Pentagon Vannevar Bush Faculty Fellowship program sponsored by the Basic Research Office of the Assistant Secretary of Defense for Research and Engineering and funded by the Office of Naval Research through Grant No. N00014-16-1-2828.

[1] U. Fano, Effects of configuration interaction on intensities and phase shifts, Phys. Rev. **124**, 1866 (1961).
[2] A. E. Miroshnichenko, S. Flach, and Y. S. Kivshar, Fano resonances in nanoscale structures, Rev. Mod. Phys. **82**, 2257 (2010).
[3] J. U. Nöckel and A. D. Stone, Resonance line shapes in quasi-one-dimensional scattering, Phys. Rev. B **50**, 17415 (1994).
[4] S. Datta, *Electronic Transport in Mesoscopic Systems* (Cambridge University Press, Cambridge, UK, 1995).
[5] T. Nakanishi, K. Terakura, and T. Ando, Theory of Fano effects in an Aharonov-Bohm ring with a quantum dot, Phys. Rev. B **69**, 115307 (2004).
[6] S. Klaiman, N. Moiseyev, and H. R. Sadeghpour, Interpretation of the Fano lineshape reversal in quantum waveguides, Phys. Rev. B **75**, 113305 (2007).
[7] R. Yang, L. Huang, Y.-C. Lai, and C. Grebogi, Quantum chaotic scattering in graphene systems, Europhys. Lett. **94**, 40004 (2011).
[8] Y. Yoon, M.-G. Kang, T. Morimoto, M. Kida, N. Aoki, J. L. Reno, Y. Ochiai, L. Mourokh, J. Fransson, and J. P. Bird, Coupling Quantum States through a Continuum: A Mesoscopic Multistate Fano Resonance, Phys. Rev. X **2**, 021003 (2012).
[9] J. Fransson, M.-G. Kang, Y. Yoon, S. Xiao, Y. Ochiai, J. L. Reno, N. Aoki, and J. P. Bird, Tuning the Fano resonance with an intruder continuum, Nano Lett. **14**, 788 (2014).
[10] I. Rotter and J. P. Bird, A review of progress in the physics of open quantum systems: Theory and experiment, Rep. Prog. Phys. **78**, 114001 (2015).
[11] L. Huang, Y.-C. Lai, H.-G. Luo, and C. Grebogi, Universal formalism of Fano resonance, AIP Adv. **5**, 017137 (2015).

[12] S. M. Reimann and M. Manninen, Electronic structure of quantum dots, Rev. Mod. Phys. **74**, 1283 (2002).
[13] F. A. Zwanenburg, A. S. Dzurak, A. Morello, M. Y. Simmons, L. C. L. Hollenberg, G. Klimeck, S. Rogge, S. N. Coppersmith, and M. A. Eriksson, Silicon quantum electronics, Rev. Mod. Phys. **85**, 961 (2013).
[14] H. G. Luo, T. Xiang, X. Q. Wang, Z. B. Su, and L. Yu, Fano Resonance for Anderson Impurity Systems, Phys. Rev. Lett. **92**, 256602 (2004).
[15] A. P. S. de Moura, Y.-C. Lai, R. Akis, J. P. Bird, and D. K. Ferry, Tunneling and Nonhyperbolicity in Quantum Dots, Phys. Rev. Lett. **88**, 236804 (2002).
[16] W. H. Zurek, Decoherence, einselection, and the quantum origins of the classical, Rev. Mod. Phys. **75**, 715 (2003).
[17] D. K. Ferry, R. Akis, and J. P. Bird, Einselection in Action: Decoherence and Pointer States in Open Quantum Dots, Phys. Rev. Lett. **93**, 026803 (2004).
[18] B. Huckestein, R. Ketzmerick, and C. H. Lewenkopf, Quantum Transport through Ballistic Cavities: Soft vs Hard Quantum Chaos, Phys. Rev. Lett. **84**, 5504 (2000).
[19] E. R. Racec, U. Wulf, and P. N. Racec, Fano regime of transport through open quantum dots, Phys. Rev. B **82**, 085313 (2010).
[20] A. A. Clerk, X. Waintal, and P. W. Brouwer, Fano Resonances as a Probe of Phase Coherence in Quantum Dots, Phys. Rev. Lett. **86**, 4636 (2001).
[21] S. Katsumoto, Coherence and spin effects in quantum dots, J. Phys.-Condens. Mat. **19**, 233201 (2007).
[22] A. Bärnthaler, S. Rotter, F. Libisch, J. Burgdörfer, S. Gehler, U. Kuhl, and H.-J. Stöckmann, Probing Decoherence through Fano Resonances, Phys. Rev. Lett. **105**, 056801 (2010).
[23] R. Yuan, R. Wang, Z. Duan, X. Song, B. Wang, and H. Yan, Mesoscopic Fano effect modulated by Rashba spin-orbit coupling and external magnetic field, Phys. Lett. A **365**, 248 (2007).
[24] M. Mendoza, P. A. Schulz, R. O. Vallejos, and C. H. Lewenkopf, Fano resonances in the conductance of quantum dots with mixed dynamics, Phys. Rev. B **77**, 155307 (2008).
[25] Y. Berlatzky and S. Klaiman, Controlling Fano profiles via conical intersections, Phys. Rev. B **79**, 085303 (2009).
[26] I. Žutić, J. Fabian, and S. Das Sarma, Spintronicsl fundamentals and applications, Rev. Mod. Phys. **76**, 323 (2004).
[27] A. Fert, Nobel lecture: Origin, development, and future of spintronics, Rev. Mod. Phys. **80**, 1517 (2008).
[28] L. G. Mourokh, V. I. Puller, A. Y. Smirnov, and J. P. Bird, Readout of single spins via Fano resonances in quantum point contacts, Appl. Phys. Lett. **87**, 192501 (2005).
[29] F. Chi, J.-L. Liu, and L.-L. Sun, Fano-Rashba effect in a double quantum dot Aharonov-Bohm interferometer, J. Appl. Phys. **101**, 093704 (2007).
[30] W. Gong, Y. Zheng, Y. Liu, F. N. Kariuki, and T. Lu, Fano effect in a T-shaped double quantum dot structure in the presence of Rashba spin-orbit coupling, Phys. Lett. A **372**, 2934 (2008).
[31] M. P. Nowak, B. Szafran, and F. M. Peeters, Fano resonances and electron spin transport through a two-dimensional spin-orbit-coupled quantum ring, Phys. Rev. B **84**, 235319 (2011).
[32] M. E. Torio, K. Hallberg, S. Flach, A.E. Miroshnichenko, and M. Titov, Spin filters with Fano dots, Eur. Phys. J. B - Cond. Matt. Complex Sys. **37**, 399 (2004).
[33] J. F. Song, Y. Ochiai, and J. P. Bird, Fano resonances in open quantum dots and their application as spin filters, Appl. Phys. Lett. **82**, 4561 (2003).
[34] V. V. Val'kov, S. V. Aksenov, and E. A. Ulanov, Spin-flip induction of Fano resonance upon electron tunneling through atomic-scale spin structures, J. Exp. Theor. Phys. **116**, 854 (2013).
[35] G.-H. Ding and B. Dong, Spin interference and the Fano effect in electron transport through a mesoscopic ring side-coupled with a quantum dot, J. Phys. Cond. Mat. **22**, 135301 (2010).
[36] R. Zhu, Spin-dependent Fano resonance induced by a conducting chiral helimagnet contained in a quasi-one-dimensional electron waveguide, J. Phys. Condens. Matter **25**, 036001 (2012).
[37] H.-H. Fu and K.-L. Yao, Spin-filter and Fano antiresonant effect in conductance through a zigzaglike polymer device: Nonequilibrium Green's function approach, J. Chem. Phys. **134**, 054903 (2011).
[38] K. P. Wójcik and I. Weymann, Perfect spin polarization in T-shaped double quantum dots due to the spin-dependent Fano effect, Phys. Rev. B **90**, 115308 (2014).
[39] Y.-C. Lai, R. Blümel, E. Ott, and C. Grebogi, Quantum Manifestations of Chaotic Scattering, Phys. Rev. Lett. **68**, 3491 (1992).
[40] R. Ketzmerick, Fractal conductance fluctuations in generic chaotic cavities, Phys. Rev. B **54**, 10841 (1996).
[41] R. P. Taylor, R. Newbury, A. S. Sachrajda, Y. Feng, P. T. Coleridge, C. Dettmann, N. Zhu, H. Guo, A. Delage, P. J. Kelly, and Z. Wasilewski, Self-Similar Magnetoresistance of a Semiconductor Sinai Billiard, Phys. Rev. Lett. **78**, 1952 (1997).
[42] A. S. Sachrajda, R. Ketzmerick, C. Gould, Y. Feng, P. J. Kelly, A. Delage, and Z. Wasilewski, Fractal Conductance Fluctuations in a Soft-Wall Stadium and a Sinai Billiard, Phys. Rev. Lett. **80**, 1948 (1998).
[43] R. Crook, C. G. Smith, A. C. Graham, I. Farrer, H. E. Beere, and D. A. Ritchie, Imaging Fractal Conductance Fluctuations and Scarred Wave Functions in a Quantum Billiard, Phys. Rev. Lett. **91**, 246803 (2003).
[44] X. Ni, L. Huang, L. Ying, and Y.-C. Lai, Relativistic quantum tunneling of a Dirac fermion in nonhyperbolic chaotic systems, Phys. Rev. B **87**, 224304 (2013).
[45] Y.-C. Lai and T. Tél, *Transient Chaos: Complex Dynamics on Finite-Time Scales* (Springer, New York, 2011).
[46] L. D. Landau and E. M. Lifshitz, *Quantum Mechanics (Non-Relativistic Theory)* (World Publishing Company, New York, 2007), 3rd ed.
[47] W. A. Lin and R. V. Jensen, Conjugate points in stadium and circle billiards, Phys. Rev. E **56**, 5251 (1997).
[48] S. Ree and L. E. Reichl, Classical and quantum chaos in a circular billiard with a straight cut, Phys. Rev. E **60**, 1607 (1999).
[49] B. K. Nikolić and S. Souma, Decoherence of transported spin in multichannel spin-orbit-coupled spintronic devices: Scattering approach to spin-density matrix from

the ballistic to the localized regime, Phys. Rev. B **71**, 195328 (2005).

[50] B. K. Nikolić and R. L. Dragomirova, What can we learn about the dynamics of transported spins by measuring shot noise in spin-orbit-coupled nanostructures?, Semicond. Sci. Tech. **24**, 064006 (2009).

[51] C.-R. Liu, X.-Z. Chen, H.-Y. Xu, L. Huang, and Y.-C. Lai, Effect of chaos on two-dimensional spin transport, Phys. Rev. B **98**, 115305 (2018).

[52] E. Joos, H. D. Zeh, C. Kiefer, D. Giulini, J. Kupsch, and I. O. Stamatescu, *Decoherence and the Appearance of a Classical World in Quantum Theory* (Springer, Berlin Heidelberg, New York, 2003).

[53] M. Schlosshauer, *Decoherence and the Quantum-To-Classical Transition* (Springer, Berlin Heidelberg, New York, 2007).

[54] J.-Y. Zeng, *Liangzi lixue. Juan II. Diwuban [Quantum Mechanics. Volume II. 5th edition]* (Kexue chubanshe, Beijing, 2014).

[55] J. Sakurai and J. Napolitano, *Modern Quantum Mechanics* (Cambridge University Press, Cambridge, 2017).

[56] R. Yang, L. Huang, Y.-C. Lai, and L. M. Pecora, Modulating quantum transport by transient chaos, Appl. Phys. Lett. **100**, 093105 (2012).

[57] R. Yang, L. Huang, Y.-C. Lai, C. Grebogi, and L. M. Pecora, Harnessing quantum transport by transient chaos, Chaos **23**, 013125 (2013).

[58] F. Mireles and G. Kirczenow, Ballistic spin-polarized transport and Rashba spin precession in semiconductor nanowires, Phys. Rev. B **64**, 024426 (2001).

[59] Y. V. Pershin and V. Privman, Low spin relaxation in two-dimensional electron systems with antidots, Phys. Rev. B **69**, 073310 (2004).

[60] C. H. Chang, A. G. Mal'shukov, and K. A. Chao, Spin relaxation dynamics of quasiclassical electrons in ballistic quantum dots with strong spin-orbit coupling, Phys. Rev. B **70**, 245309 (2004).

[61] F. Zhai and H. Q. Xu, Symmetry of Spin Transport in Two-Terminal Waveguides with a Spin-Orbital Interaction and Magnetic Field Modulations, Phys. Rev. Lett. **94**, 246601 (2005).

[62] G. B. Akguc and J.-B. Gong, Spin-dependent electron transport in two-dimensional waveguides of arbitrary geometry, Phys. Rev. B **77**, 205302 (2008).

[63] L. Ying and Y.-C. Lai, Enhancement of spin polarization by chaos in graphene quantum dot systems, Phys. Rev. B **93**, 085408 (2016).